Polymer chain dynamics in intercalated poly(epsilon-caprolactone)/nanoplatelet mixtures

Kevin A. Masser,[†] Hongyi Yuan,[‡] Alamgir Karim,[‡] and Chad R. Snyder[*,†]

Polymers Division, National Institute of Standards and Technology, Gaithersburg, MD 20899, and Department of Polymer Engineering, The University of Akron, Akron, OH 44325

E-mail: chad.snyder@nist.gov

Abstract

The dynamics of poly(ε-caprolactone) (PCL) blends with small amounts of Cloisite 30B nanoplatelets were investigated via broadband dielectric relaxation spectroscopy. The terminal relaxation, or normal mode of PCL, was found to be strongly influenced by the presence of the nanoplatelets, exhibiting a relaxation from PCL chains within the Cloisite platelets as well as a bulk-like relaxation. These results, as well as X-ray scattering and rheological results from the literature, help to form a clearer picture of how the structure and dynamics relate to the bulk physical properties in these systems. Cloisite was observed to have minimal impact on both the glassy state dynamics as well as the segmental dynamics, due to the relatively weak interactions between the polymer and the platelets. Official contribution of the National Institute of Standards and Technology; not subject to copyright in the United States.

Nanobiocomposites hold great potential due to their inherent biodegrability and lack of impact on the environment, which enable a myriad of short-term applications ranging from medical products to food packaging.[1] Two of the most highly researched components for nano-biocomposites

---

[*]To whom correspondence should be addressed
[†]NIST
[‡]University of Akron

are poly(ε-caprolactone) (PCL) and montomorillonite-based nanoclays. The extensive continuing research on these components, however, shows our lack of complete understanding of these materials. This lack of fundamental understanding stems from the difficulties associated with the large number of components (i.e., polymer(s), nanoclay, possible additives and clay surface modifiers), the semicrystalline nature of the polymer, and the interactions between all the components and their impact on nanoclay dispersion and the polymer crystallization process.

For most of the envisioned applications of these nano-biocomposites, the mechanical properties are some of the most important design parameters. At the heart of most of the mechanical properties lie the polymer chain dynamics and the impact of the nanoclay on those dynamics. Previous investigations of the mechanical properties of PCL have observed two interesting phenomena: an increase in the complex viscosity (η^*)[2] and a concurrent increase in the activation energy associated with the longest relaxation time[3] upon addition of Cloisite 30B,[4] a methyl, tallow, bis-2-hydroxyethyl, quaternary ammonium salt functionalized montmorillonite clay, having platelets approximately 5 μm in diameter. Complementing the results of these studies are measurements from solid state nuclear magnetic resonance (NMR) spectroscopy that suggest changes in chain dynamics due to intercalation into saponite platelets[5,6] and molecular dynamics (MD) simulations[7] that propose an increase in conformational order on intercalation between montmorillonite platelets. Unfortunately, the NMR studies were for clay mass fractions of greater than 50 %, far above the 10 % or less typically used in nanocomposites, and neither the NMR or MD simulations captured the temperature dependence of these features and hence no insight into the activation energies for the processes.

In this study, the dynamics of semicrystalline PCL with Cloisite 30B are investigated via broadband dielectric relaxation spectroscopy. PCL belongs to a somewhat rare class of Normal Mode, or type-A, polymers,[8–11] which contain a molecular dipole oriented along the chain axis. This type of dipole allows the relaxation behavior of the longest relaxation time (tube disengagement or terminal relaxation) to be investigated. This characteristic is beneficial for broadband dielectric relaxation spectroscopy studies, by allowing the effects of confinement and specific interactions on

the glassy state (β relaxations), the glass transition (the segmental or α relaxation) and the longest relaxation time to be investigated. It has been shown that PCL intercalates clay platelets[12] via solvent intercalation in chloroform. It should be noted that previous studies have examined the effects of nanoplatelets in PCL,[2,3,13–15] but changes in the terminal relaxation time (longest relaxation time) have not been investigated. The terminal relaxation time is perhaps, along with the viscosity, the most important characteristic in polymer and polymer nanocomposite processing. Understanding the effects of filler on the terminal relaxation is critical for process design. The present paper focuses on the dielectric measurements of the terminal relaxation time in the presence of organically modified clay to deconvolute out the effects of polymer crystallization, clay concentration, and intercalation on polymer chain dynamics.

Experimental Section

Poly(ε-caprolactone) was obtained from Sigma-Aldrich and used without further purification, having a number average molar mass of $\approx$80,000 g/mol. Appropriate amounts of Cloisite 30B clay (Southern Clay Products), as well as PCL were weighed to create (2, 4 and 6) % mass fraction Cloisite 30B samples, which were then dissolved in toluene. The (2 to 3) % by mass solutions were then ultrasonicated in a B2500A-MTH Ultrasonics cleaner for two hours to facilitate dispersion. The number in the sample designations (PCL0, PCL2, PCL4, PCL6) refers to the % mass fraction of Cloisite 30B.

Differential Scanning Calorimetry (DSC) was performed on a Perkin Elmer DSC 8500, with a liquid nitrogen chiller and helium purge gas. Indium, lead, and cyclohexane were used as temperature calibration standards, and indium was used as a heat flow standard. Samples were heated to 100 °C for 2 min to erase thermal history. Two separate runs were performed, one at 10 °C/min and one at 0.25 °C/min, to mimic the dielectric measurements. Subsequent heating scans at 10 °C/min were performed after each of these cooling measurements. The enthalpies of fusion/crystallization for the PCL samples were calculated by integrating the melting endotherm and crystallization

exotherms with a sigmoidal baseline. The measured enthalpies were converted to mass fraction crystallinity by first correcting for the mass fraction of the clay and then dividing by the heat of fusion of a pure PCL crystal (17.9 J/mol) obtained from the ATHAS database.[16] The glass transition for all heating traces was defined as the point halfway between the extrapolated glass and melt/semicrystalline heat capacities.

Wide-Angle X-Ray Scattering (WAXS) was performed on a D8 Discover X-ray diffractometer (Bruker) using a Cu-Kα X-ray source with a wavelength of 1.5418 Å. The Cloisite 30B sample was prepared by confining a small amount of Cloisite particles in the window of the WAXS sample stage using adhesive tape. The obtained spectrum was then corrected by subtracting the spectrum of the adhesive tape. Homopolymer and nanocomposite samples were prepared by drop-casting their solutions on UV ozone treated glass slides. After solvent evaporation, samples were rinsed with deionized water and peeled off the glass slides. Samples were then placed in a vacuum chamber at room temperature for 30 mins, then attached to the sample stage for WAXS.

Parallel plate capacitor samples for dielectric spectroscopy measurements were drop cast from solution directly onto 20 mm diameter brass electrodes. After toluene evaporation, the samples were dried in an oil free vacuum oven above the melting temperature of PCL ($\approx$60 °C) and well below the degradation temperature,[17] for a minimum of 10 h. After cooling to room temperature, two silica spacers, 40 µm in diameter, were placed onto the film along with a 10 mm diameter brass electrode. The entire assembly was clamped together and returned to the vacuum oven well above the melting temperature of PCL for (3 to 4) h to imbed the upper electrode into the film, after which, the sample was allowed to slowly cool to room temperature. The resulting film thickness was controlled by the silica spacers at 40 µm. Samples were quickly transferred to the nitrogen cryostat of the impedance analyzer to avoid moisture absorption, which has been shown to strongly alter the dynamics of PCL[18] and polymeric systems in general, even at low water content.[19]

The complex dielectric constant [$\varepsilon^*(\omega) = \varepsilon'(\omega) - i\varepsilon''(\omega)$] was measured via dielectric relaxation spectroscopy, performed on a Concept 40 Novocontrol Alpha impedance analyzer, manufactured by Novocontrol Technologies GmbH. A frequency range of 10 MHz to 10 mHz was

investigated from 150 °C to -140 °C. The manufacturer's stated accuracy of the Alpha analyzer is between (0.1 and 1) % for the sample capacitance used over the given frequency range. Temperature was controlled with a Quatro cryostat, which heats gas from a liquid nitrogen dewar with a temperature setpoint accuracy of 0.1 °C. All samples were measured every five degrees on cooling, then every ten degrees on heating, with a 10 min stabilization time after the sample was within 0.5 °C of the setpoint. No differences between the cooling and heating scans were observed, so only the data from cooling are shown. Note that the lack of expected difference in relaxation behavior in the crystallization region is due to the fact that measurements on heating were performed at 10 °C steps versus 5 °C for cooling, with each temperature requiring 30 min to collect.

The isothermal dielectric loss was modeled with a Havriliak-Negami function.[20]

$$\varepsilon'' = \frac{\Delta\varepsilon}{[1+(i\omega\tau)^n]^m} + \frac{\sigma_\circ}{\varepsilon_\circ \omega^s} \tag{1}$$

$\Delta\varepsilon = \varepsilon_s - \varepsilon_\infty$ is the dielectric strength, and is related to the number density of dipoles involved in the observed relaxation, as well as the magnitude of their dipole moment and how they are correlated.[11,21] ε_s and ε_∞ are the zero frequency and infinite frequency dielectric constants, respectively. τ is the relaxation time, n is the relaxation breadth and m is the high frequency asymmetry, both having a value between 0 and 1. ω is the angular frequency. The second term of equation (Eq. (1)) accounts for dc conductivity ($\sigma_\circ$, when present). $\varepsilon_\circ$ is the permittivity of vacuum (8.854 pF/m), and s is an adjustable parameter. From these fitting parameters, the relaxation frequency (f_{Max}) is calculated via:

$$f_{Max} = \frac{1}{2\pi\tau} \left[\frac{sin\left(\frac{\pi n}{2+2m}\right)}{sin\left(\frac{\pi nm}{2+2m}\right)} \right]^{1/n} \tag{2}$$

In the case of the normal mode, the conductivity-free loss was modeled using a methodology developed by Wübbenhorst.[22] The derivative of the dielectric constant is used, and this approximates the conductivity-free dielectric loss. In these cases, a 'derivative HN' function must be used (see reference 22 for details).

5

The glassy-state, or β relaxation of PCL was fit with an Arrhenius function.[11]

$$f_{Max} = f_\circ \exp\left(\frac{-E_a}{RT}\right) \qquad (3)$$

In equation (Eq. (3)), $f_\circ$ is the Arrhenius prefactor, E_a is the activation energy, R is the universal gas constant, and T is the temperature. The temperature dependence of the segmental relaxations was modeled with a Vogel-Fulcher-Tammann (VFT) function.

$$f_{Max} = f_\circ \exp\left(\frac{-B}{T - T_\circ}\right) \qquad (4)$$

In equation (Eq. (4)), $f_\circ$ is the VFT prefactor, B is an adjustable parameter related to the dynamic fragility, and $T_\circ$ is the Vogel temperature.

Results and Discussion

The systems examined in this manuscript provide the ability to gain deep insight into the molecular motions in PCL by comparing dynamics, both without nanoclay and with varying levels of it added, (1) in the melt where PCL is amorphous, but intercalated into the clay, and (2) in the glassy regime where PCL is semicrystalline. PCL exhibits three relaxations in the temperature/frequency range investigated: a glassy state β relaxation, a segmental α relaxation related to the dynamic glass transition temperature (T_g) of the polymer, and a normal mode relaxation, which is related to the terminal relaxation time of the polymer. Other normal mode semicrystalline polymers, such as 1,4-trans polyisoprene exhibit an additional segmental relaxation upon crystallization, due to the presence of constrained chains, or the so-called rigid amorphous fraction.[23,24] While PCL possesses a rigid amorphous fraction,[25] it does not exhibit an additional relaxation due to the rigid amorphous fraction.[18]

In this article, the number after PCL (0, 2, 4, 6) indicates the mass % of Cloisite 30B clay. Shown in Figure 1 (a) and (b) is the dielectric loss as a function of temperature on cooling for the

PCL series. At low temperatures ($T < T_g$), PCL exhibits a local (β) relaxation. At higher temperatures, the dynamic T_g (α, or segmental) is present. At higher temperatures still, the normal mode appears as a weak shoulder on the large contribution from mobile ionic species, which typically results in dielectric loss values many orders of magnitude greater than the dipolar relaxations of interest.[11] These general features agree well with the literature.[18,26]
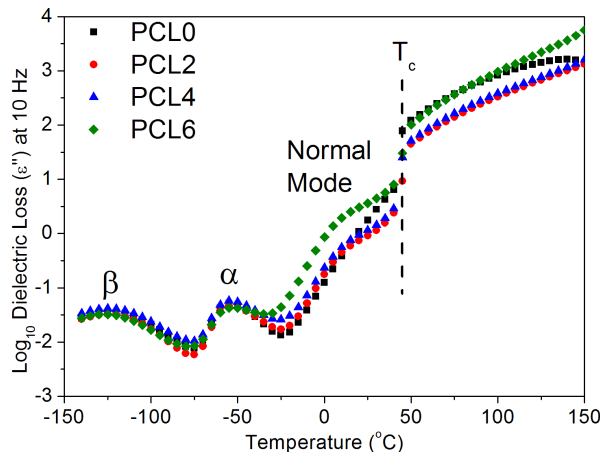

Figure 1: Poly(ε-caprolactone) (PCL) relaxation behavior. Typical values of dielectric loss as a function of temperature for the PCL series at 10 Hz. Approximate locations of relaxations are indicated on the plot, as well as the average crystallization temperature (T_c) for the cooling rate used.

Shown in Figure 2 is an Arrhenius plot of the relaxation frequencies of the PCL normal mode at the different nanoplatelet loadings studied. The neat PCL (PCL0) relaxation behavior (open black squares in Figure 2) exhibits a typical VFT-like temperature dependence until the effective crystallization temperature, at which point the terminal relaxation is restricted by the presence of PCL crystals, causing a dramatic increase in relaxation time for the remaining amorphous PCL chains. The crystalline portion of PCL can not contribute to the observed relaxation. The onset of crystallization, measured by DSC, was found to be (45 ± 1) °C[27] at a cooling rate similar to that used in DRS experiments. In addition to an increase in relaxation time, an increase in the relaxation strength (see Figure 3) is also observed upon crystallization. This is expected, since the remaining amorphous PCL chains likely exist in a more extended conformation as tie chains between crystals, resulting in a net larger dipole moment.
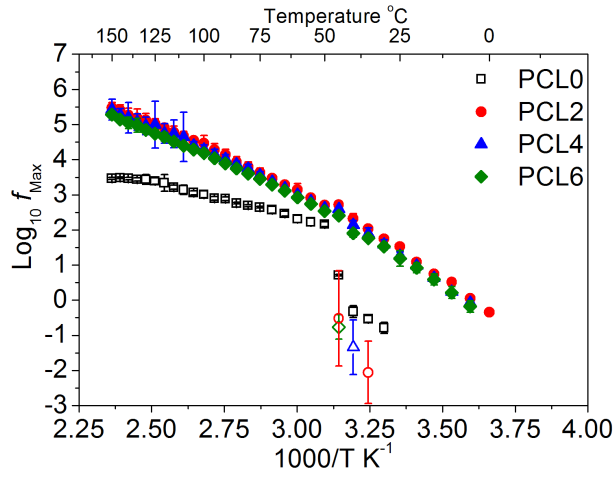
7

Figure 2: Arrhenius plot of the PCL normal mode. The relaxation frequencies (frequency $\propto$ 1/time) of the PCL normal mode within the Cloisite platelets (filled symbols) and the relaxation of bulk-like PCL (open symbols) in an Arrhenius-type plot. (Note that the error bars in all plots correspond to estimates of one standard deviation in the experimental uncertainty, as derived from the covariance matrix of the fits.)
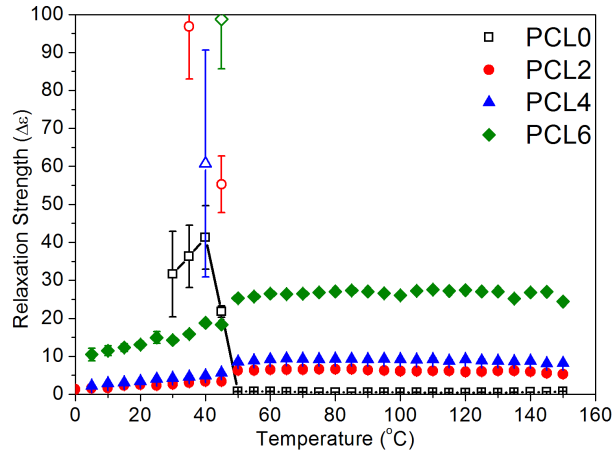

Figure 3: PCL normal mode relaxation strength. Relaxation strength ($\Delta\varepsilon$) versus temperature for the normal mode of the PCL series of nanocomposites. The relaxation of PCL within the Cloisite platelets (filled symbols) and the relaxation of bulk-like PCL (open symbols) are shown. The solid line for PCL0 is a guide for the eye.

At all nanoplatelet compositions, two relaxations are observed in the temperature range where the normal mode is in the frequency window of the spectrometer. One relaxation at higher frequencies compared to the bulk (filled symbols in Figure 2), and another which has relaxation frequencies comparable to the bulk (open symbols in Figure 2). Due to the strong overlap of the two processes at higher temperatures, and the low relaxation intensity of the bulk-like relaxation (see Figure 3), the bulk-like relaxation times could only be modeled at temperatures below the effective crystallization temperature, where the abrupt slowdown in dynamics due to bulk crystallization allows for accurate modeling of both processes. The temperature dependence of the normal mode relaxations in PCL2, PCL4 and PCL6 are the same in each system, but the relaxation strength of the higher frequency process increases with nanoplatelet loading. Additionally, as observed in Figure 2, the activation energy of the fast process is greater than the slow process. The increase in relaxation strength with nanoplatelet composition without changes in the relaxation frequency suggests the process is in some way related to the Cloisite nanoplatelet content. X-ray scattering results, discussed further below, confirm the presence of PCL within the Cloisite galleries (see Figure 4). Below the crystallization temperature, a small decrease in relaxation strength is observed for the higher frequency process and a large increase in the relaxation strength is observed for the lower frequency process. This subtle decrease with temperature of the higher frequency process relaxation strength indicates the motion responsible for this process persists, nearly unchanged, below the crystallization temperature. This is supported by the fact that the relaxation frequency of the high frequency process exhibits no change in temperature dependence upon crystallization. The lower frequency process follows a qualitatively similar temperature dependence to the bulk PCL sample, suggesting this motion is the same as observed in bulk PCL.

Considering these observations, the following physical interpretation is proposed: The high frequency process arises from the terminal relaxation of PCL chains intercalated within the Cloisite nanoplatelets. The low frequency process is the bulk-like PCL terminal relaxation. Thin film PCL crystallization studies reveal that at thicknesses near the radius of gyration ($\approx$6 nm), PCL does not crystallize.[28] X-ray scattering results (see Figure 4) indicate the Cloisite gallery spacing increases
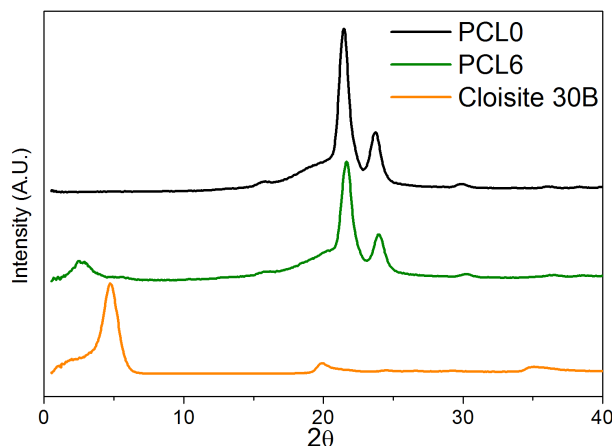
Figure 4: Representative X-ray scattering results for neat PCL (black line - top), PCL with 6 mass % Cloisite 30B (green line - middle) and neat Cloisite 30B (orange line - bottom). Data have been offset for clarity.

from ≈1.8 nm (the peak at ≈ 4, 2θ) to ≈3.6 nm (the peak at ≈ 2, 2θ), well below the radius of gyration of PCL, suggesting PCL cannot crystallize within the Cloisite platelets. As the Cloisite composition is increased, a greater volume fraction of the sample exists within the platelets, resulting in a proportionally larger relaxation strength. The slight decrease in relaxation strength of the high frequency process upon PCL crystallization may be due to crystallization from the nanoplatelet surface, restricting the motion of the PCL chains on the nanoplatelet surfaces. It may also be due to the crystallization of chains which are only partially intercalated in the ≈5 μm diameter Cloisite discs. DSC and optical microscopy results suggests that although the number of crystals in the nanocomposite samples is greater than in neat PCL, i.e., higher nucleation density, the overall percentage crystallinity may have decreased slightly from ≈59 % (see Supplemental Information for crystallinity) for neat PCL, to ≈56 % for the nanocomposites, but this possible change is within the statistical uncertainty of the measurements. This is also consistent with previous studies on the crystallization kinetics in this system.[29] A correlation between the possible reduction in crystallinity and the increase in the relaxation strength of the new normal mode is not likely possible, since the precise volume fraction of intercalated PCL chains would need to be known, as well as any changes in the distributions in the dipole moment of the end-to-end dipole.[30]

The increase in relaxation frequency (decrease of relaxation time) and the increase in the temperature dependence (activation energy) of the high frequency process is likely due to disentanglement of the PCL chains as they intercalate between the Cloisite layers. An alternative explanation for the increase in relaxation frequency would be a reduction in molar mass of PCL, as a molar mass reduction has been shown to affect the normal mode relaxation time.[9] This is unlikely, because a broadening of the segmental relaxation and a lowering of T_g would be expected in the case of chain scission.

The relaxation behavior of these nanocomposites are in agreement with rheological data on these systems published previously,[3] which showed an increase in the complex viscosity and an increase in the activation energy associated with the terminal relaxation time with the addition of Cloisite. The physical mechanism of these observed changes is now clear; the increase in the activation energy associated with the terminal relaxation time observed in rheological data is a result of the faster relaxation of PCL chains within the Cloisite platelets, a phenomenon commonly observed in antiplasticized systems. The increased viscosity is simply due to the presence of the rigid nanoplatelets,[31] and the additional relaxation strength ($\Delta\varepsilon = \varepsilon_s - \varepsilon_\infty$, see Figure 3) caused by the presence of intercalated PCL chains, which has been related to the complex viscosity.[32]

The effects of clay intercalation on the cooperative segmental dynamics and local dynamics was also investigated. The segmental relaxation of the PCL series is unaffected by the addition of nanoplatelets, as shown in Figure 1 and Figure 5. This is confirmed by the DSC results which show no changes in the glass transition temperature with the addition of Cloisite. All PCL nanocomposites exhibit a T_g of (-60 $\pm$ 2) °C.

Vogel-Fulcher-Tammann (VFT) fits were performed (see Experimental section for fit functions). $f_\circ$ was fixed at 10^{13} Hz, B has a value of (820 $\pm$ 50) K, and a Vogel temperature of (188 $\pm$ 10) K. The VFT prefactor ($f_\circ$) was fixed due to the unusual temperature dependence of the segmental relaxation and due to the relatively strong β relaxation merging with the segmental relaxation at higher temperatures. Calculating the temperature at a relaxation time of 100 s provides an accurate estimation of T_g determined by calorimetric methods.[11] The calculated T_g is (-63 $\pm$ 5) °C
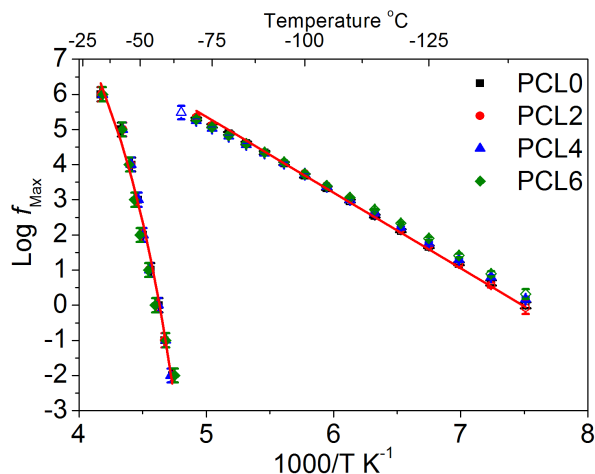
Figure 5: Arrhenius plot for the PCL segmental relaxation, also known as the dynamic T_g (filled symbols), and the glassy state β relaxation (open symbols). Solid lines are representative Vogel-Fulcher-Tammann fits to the segmental relaxation and Arrhenius fits to the β relaxation.

for every sample, in agreement with the DSC-determined T_g. No statistically significant changes in either the breadth (n from equation (Eq. (1))) or the asymmetry parameter (m from equation (Eq. (1))) were observed for any of the samples, indicating the distribution of relaxation times for the dynamic T_g is constant at every nanoplatelet composition studied.

As with the segmental relaxation, the temperature dependence of the β relaxation of the PCL series is unaffected by clay content (see Figure 5). The β relaxation maintains an average activation energy of (38 ± 2) kJ/mol, and an Arrhenius prefactor (f_o) of $10^{(15\pm0.1)}$ Hz. The lack of changes in the temperature dependence of the β and α relaxations in these systems suggests that, while favorable, the hydrogen bonds formed between the carbonyl groups of PCL with the Cloisite functionality are rather weak.[33] It has been observed that weak hydrogen bonds have been shown to have little effect on local dynamics when compared to strong hydrogen bonds.[34]

Conclusion

The relaxation behavior of a series of nanocomposites based on Cloisite 30B with a normal mode polymer, poly(ε-caprolactone) (PCL) was investigated via broadband dielectric relaxation spec-

troscopy, optical microscopy, differential scanning calorimetry and X-ray scattering. PCL's glassy state (β) relaxation was found to be unaffected by the presence of the nanoplatelets, as was the dynamic glass transition, or segmental (α) relaxation. The normal mode (terminal relaxation) of PCL was strongly affected by the addition of Cloisite nanoplatelets. At all loadings, a second, higher frequency normal mode relaxation was observed, which is assigned to motion of PCL chains within the Cloisite nanoplatelets. The bulk-like PCL normal mode relaxation appears to be largely unaffected by the presence of nanoplatelets, although its overall contribution to the system dynamics is reduced. The observed effects of Cloisite loading mirrors the effects observed rheologically in the literature, and provides deeper insight into the unusual terminal flow character of these systems. The additional stress relaxation mechanism provided by the faster PCL relaxation within the Cloisite platelets may have a profound impact on the industrial-level processing of such nanocomposites.

Acknowledgement

Supporting Information Available: Polarized optical micrographs of each system, and calculated percentage crystallinity. This material is available free of charge *via* the Internet at http://pubs.acs.org

Supplemental Information

Polarized optical micrographs, collected in transmission mode using a 20X objective, are shown in Figure 6. While negligible changes in the total crystallinity are observed with differential scanning calorimetry, the number density of crystals is greater in each of the nanocomposites compared to neat poly(ε-caprolactone).
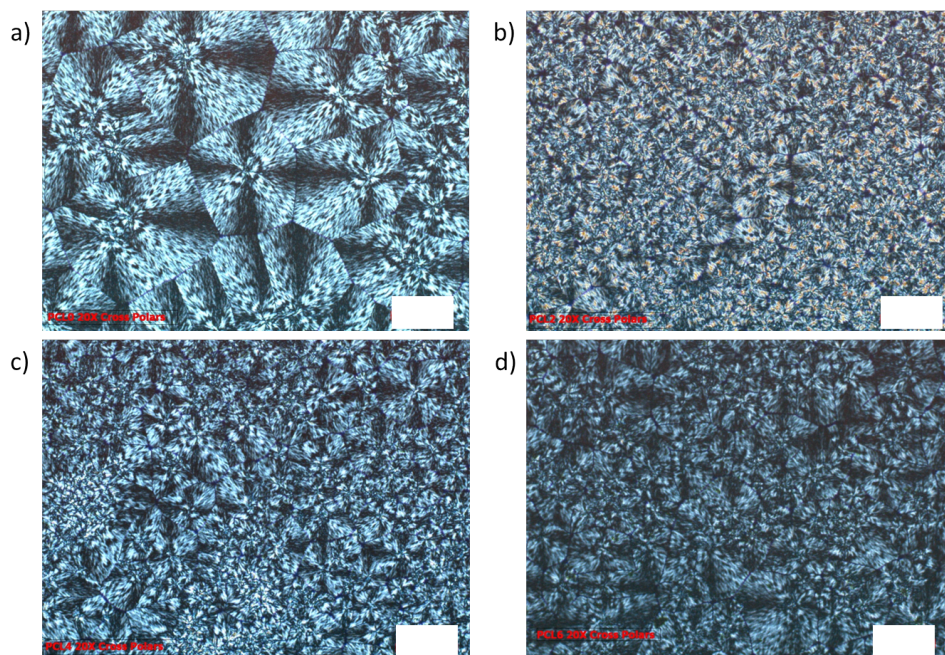
Figure 6: Cross polarized optical microscope images of PCL (a), PCL2 (b), PCL4 (c) and PCL6 (d). The white bars in each image indicate 100 μm.

The percentage crystallinity, calculated from DSC data, are shown in Figure 7. A small decrease in total crystallinity is observed, but this decrease is less than the standard deviation of the measurement/calculation.
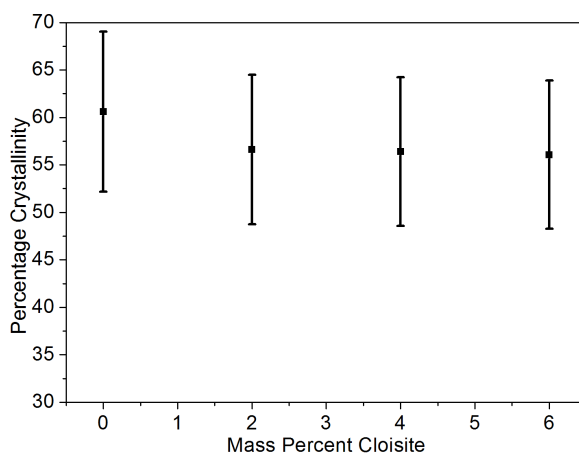

Figure 7: Mass fraction crystallinity as a function of Cloisite content.

14

Notes and References

(1) Bordes, P.; Pollet, E.; Avérous, L. *Progress in Polymer Science* **2009**, *34*, 125–155.

(2) Block, C.; Watzeels, N.; Rahier, H.; Van Mele, B.; Van Assche, G. *Journal of Thermal Analysis and Calorimetry* **2011**, *105*, 731–736.

(3) Chung, J. W.; Oh, K. S.; Kwak, S. Y. *Macromolecular Materials and Engineering* **2007**, *292*, 627–633.

(4) *Certain commercial equipment, instruments, or materials are identified in this paper in order to specify the experimental procedure adequately. Such identification is not intended to imply recommendation or endorsement by the National Institute of Standards and Technology, nor is it intended to imply that the materials or equipment identified are necessarily the best available for the purpose.*

(5) Hrobarikova, J.; Robert, J.-L.; Calberg, C.; Jérôme, R.; Grandjean, J. *Langmuir* **2004**, *20*, 9828–9833.

(6) Urbanczyk, L.; Hrobarikova, J.; Calberg, C.; Jérôme, R.; Grandjean, J. *Langmuir* **2006**, *22*, 4818–4824.

(7) Gardebien, F.; Gaudel-Siri, A.; Brédas, J.-L.; Lazzaroni, R. *J. Phys. Chem. B* **2004**, *108*, 10678–10686.

(8) Stockmayer, W. H. *Pure and Applied Chemistry* **1967**, *15*, 539–554.

(9) Adachi, K.; Imanishi, Y.; Kotaka, T. *Journal Of The Chemical Society-Faraday Transactions I* **1989**, *85*, 1065–1074.

(10) Adachi, K.; Kotaka, T. *Progress in Polymer Science* **1993**, *18*, 585–622.

(11) Kremer, F.; Schonhals, A. *Broadband Dielectric Spectroscopy*, 1st ed.; Springer-Verlag: New York, 2003.

(12) Jimenez, G.; Ogata, N.; Kawai, H.; Ogihara, T. *Journal of Applied Polymer Science* **1997**, *64*, 2211–2220.

(13) Gorrasi, G.; Tortora, M.; Vittoria, V.; Galli, G.; Chiellini, E. *Journal of Polymer Science Part B-Polymer Physics* **2002**, *40*, 1118–1124.

(14) Homminga, D.; Goderis, B.; Dolbnya, I.; Groeninckx, G. *Polymer* **2006**, *47*, 1620–1629.

(15) Miltner, H. E.; Watzeels, N.; Block, C.; Gotzen, N. A.; Van Assche, G.; Borghs, K.; Van Durme, K.; Van Mele, B.; Bogdanov, B.; Rahier, H. *European Polymer Journal* **2010**, *46*, 984–996.

(16) Pyda, M. Advanced THermal Analysis System.

(17) Sivalingam, G.; Madras, G. *Polymer Degradation and Stability* **2004**, *84*, 393–398.

(18) Grimau, M.; Laredo, E.; Perez, M. C. Y.; Bello, A. *Journal of Chemical Physics* **2001**, *114*, 6417–6425.

(19) Cerveny, S.; Alegria, A.; Colmenero, J. *Physical Review E* **2008**, *77*, 0318031–0318035.

(20) Havriliak, S.; Negami, S. *Polymer* **1967**, *8*, 161–210.

(21) Onsager, L. *Journal Of The American Chemical Society* **1936**, *58*, 1486–1493.

(22) Wübbenhorst, M.; van Turnhout, J. *Journal of Non-Crystalline Solids* **2002**, *305*, 40–49.

(23) McCrumb, N.; Read, B.; Williams, G. *Anelastic and Dielectric Effects in Polymeric Solids*; Dover Publications: New York, 1967.

(24) Cerveny, S.; Zinck, P.; Terrier, M.; Arrese-Igor, S.; Alegría, A.; Colmenero, J. *Macromolecules* **2008**, *41*, 8669–8676.

(25) Wunderlich, B. *Progress in Polymer Science* **2003**, *28*, 383–450.

(26) Pluta, M.; Jeszka, J. K.; Boiteux, G. *European Polymer Journal* **2007**, *43*, 2819–2835.

(27) All reported uncertainties in experimental values are the best estimate of 1 standard deviation in the experimental uncertainty. Uncertainties in fit parameters were obtained in the normal manner through use of the covariance matrix of the fit.

(28) Qiao, C.; Zhao, J.; Jiang, S.; Ji, X.; An, L.; Jiang, B. *Journal of Polymer Science Part B: Polymer Physics* **2005**, *43*, 1303–1309.

(29) Di Maio, E.; Iannace, S.; Sorrentino, L.; Nicolais, L. *Polymer* **2004**, *45*, 8893–8900.

(30) Froltsov, V. A.; Klapp, S. H. L. *The Journal of Chemical Physics* **2006**, *124*, 134701.

(31) Bicerano, J.; Douglas, J. F.; Brune, D. A. *Journal of Macromolecular Science, Part C: Polymer Reviews* **1999**, *39*, 561–642.

(32) DiMarzio, E. A.; Bishop, M. *The Journal of Chemical Physics* **1974**, *60*, 3802–3811.

(33) Coleman, M. M.; Graf, J.; Painter, P. C. *Specific Interactions and the Miscibility of Polymer Blends*, 1st ed.; Technomic Publishing Company: Lancaster, 1991.

(34) Masser, K. A.; Zhao, H.; Painter, P. C.; Runt, J. *Macromolecules* **2010**, *43*, 9004–9013.

Graphical TOC Entry

For Table of Contents Use Only Polymer chain dynamics in intercalated poly(epsilon-caprolactone)/nanoplatelet mixtures Kevin A. Masser, Hongyi Yuan, Alamgir Karim, Chad R. Snyder